Bulletin of Earthquake Engineering (2020) 18:5009–5029
https://doi.org/10.1007/s10518-020-00886-0

ORIGINAL RESEARCH

Influence of wood infill walls on the seismic performance of Chinese traditional timber structure by shaking table tests

Qifang Xie[1,2] · Long Wang[1,3] · Shengying Li[1,2] · Lipeng Zhang[1,2] · Weibing Hu[1]

Received: 1 June 2019 / Accepted: 2 June 2020 / Published online: 10 June 2020

Abstract
Wood infill walls have significant effect on the seismic performance of Chinese traditional timber structure. Based on cyclic tests of wood infill walls, a 1:6 scaled traditional timber structure, one direction with wood infill walls and the other direction without ones, were fabricated and subjected to artificial and recorded earthquake waves through shaking table tests. The dynamic characteristics, dynamic responses and energy dissipation in the two directions were comparatively discussed to quantify the contribution of wood infill walls. The test results indicated that the natural frequencies of the model with wood infill walls was much greater than that without ones, increased more than 25%, while the increase of damping ratio was relatively insignificant before experiencing earthquakes. And the acceleration responses of the structure incorporating wood infill walls were moderately increased due to the additional lateral stiffness provided by wood infill walls, while the displacement responses dramatically decreased, especially under strong earthquakes. In addition, the wood infill walls effectively decreased the proportion of plastic strain energy in total energy, which can contribute to reduce structural damage.

Keywords Chinese traditional timber structure · Wood infill walls · Shaking table test · Dynamic characteristics · Dynamic responses · Energy dissipation

1 Introduction

Timber structure is the most characteristic one in Chinese traditional architectures. Most have endured earthquakes without collapsing many times in more than a thousand years. The thick column (Suzuki and Maeno 2006; He and Wang 2018; Qin and Yang 2018), mortise-tenon joint (King et al. 1996; Chang et al. 2009, 2017; Chen et al. 2016) and

✉ Qifang Xie
xieqfgh@xauat.edu.cn

1 School of Civil Engineering, Xi'an University of Architecture and Technology, Xi'an 710055, Shaanxi, China

2 Key Laboratory of Structure Engineering and Earthquake Resistance, Xi'an University of Architecture and Technology, Xi'an 710055, Shaanxi, China

3 China Jikan Research Institute of Engineering Investigations and Design, Co., Ltd., Xi'an 710043, Shaanxi, China

Dou-Gong (D'Ayala and Tasi 2008; Wu et al. 2018b), are considered to be the primary resisting elements in traditional timber structures due to the collaborative work of embedment, shearing and friction (Kitamor et al. 2010; Yeo et al. 2016). However, frames consisted of these elements are low in lateral stiffness and large in deformation (Katagihara 2001; Shi et al. 2018; Yeo et al. 2018; Xie et al. 2020a, b).

Recently, more and more attentions have been paid to the infill walls as they not only can contribute to increase the lateral stiffness and strength but also be an efficient source of energy dissipation (Benavent-Climent et al. 2018; Yuan 2018). Various traditions, climates, and territorial situations result in different materials for infill walls all over the world. Studies have been conducted on contributions of stone, masonry, and earth (mud) infill (Tsuwa and Koshihara 2012; Branco et al. 2014; Vieux-Champagne et al. 2014; Dutu et al. 2015; Xu et al. 2015). As wood infill walls are commonly used in Chinese traditional timber structures, researches on mechanical properties of structures with wood infill walls have also been carried out. Chang et al. (2007a; b) proved that embedment between wood infill walls and timber frames dominated the deformation resisting earthquakes. Crayssac et al. (2018) experimentally demonstrated that wooden panels infill significantly improved the load carrying capacity, lateral stiffness and energy dissipation capacity for traditional timber structure. However, these researches are mainly focused on static tests, and few dynamic researches on traditional timber structure with wood infill walls have been reported.

In order to specifically clarify the influence of wood infill walls on the seismic performance of traditional timber structures in term of dynamics, shaking table tests are useful and indispensable. This study conducted shaking table tests on a 1:6 scaled traditional timber structure, one direction with wood infill walls and the other direction without ones. By comparative analyses, the contributions of wood infill walls were quantified in terms of dynamic characteristics, dynamic responses and energy dissipation capacity.

2 Preliminary test

The major tests were conducted on a scaled traditional timber structure by shaking table. Before carrying out the complex shaking table tests, preliminary tests of structural element (wood infill wall) should be implemented to understand the mechanical behaviors.

Two specimens (as shown in Fig. 1), which took the wood infill walls installed on the first and second storeys of shaking table test model as prototype, respectively, were tested in the low cyclic loading tests. The wood infill walls were made by wood-based composite boards with a thickness of 18 mm. Other detailed geometric dimensions are shown in Fig. 1. The averaged modulus of elasticity, compressive strength and the corresponding coefficients of variation (in parentheses) of the composite wood were 12,277 MPa (0.13) and 21.7 MPa (0.09), respectively.

Figure 2 shows the test setup with one of the specimens. The restrained timber beam at the bottom was fixed to the bottom steel beam by L-shaped steel to prevent the exterior timber frame from having uplift and lateral movement. Meanwhile, the out-of-plane behaviors of the exterior timber frame were also avoided by a side support system with H-shaped steel beams, on which pulleys were attached allowing the exterior timber frame to travel in horizontal direction, at both lateral sides of the restrained timber beam at the top. In addition, mortise-tenon joints connecting beams and columns were replaced by bolted connections to eliminate the effect of joint stiffness of the exterior timber frame. And the

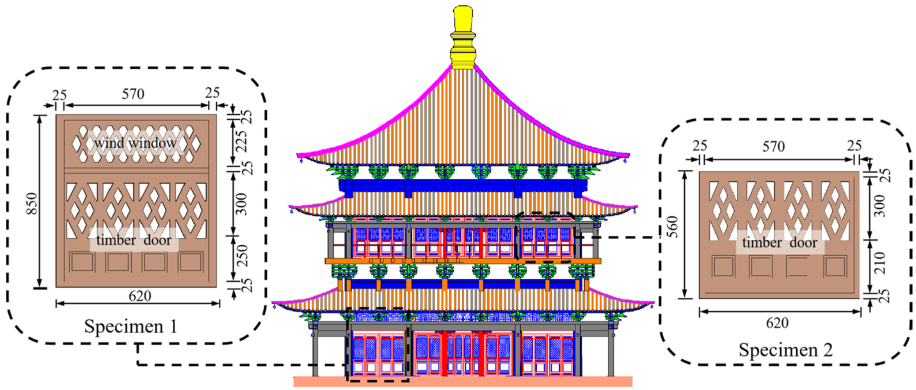

Fig. 1 Shaking table test model with wood infill walls

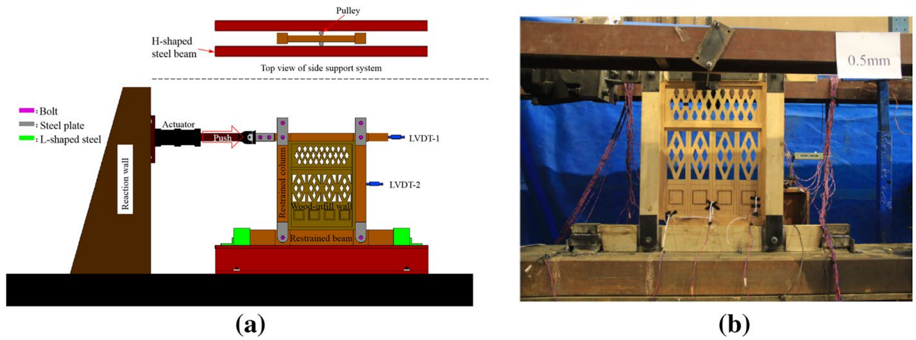

Fig. 2 Test setup for cyclic test (specimen 1): **a** Sketch of the test setup; and **b** photo of the test specimen. LVDT is linear variable differential transformer, which is used to measure lateral displacement

wood infill walls were connected to the exterior timber frame only by extrusion and friction without any connecting members. So the rocking behaviors of the exterior timber frames no longer provided any reaction forces and the force measured by cyclic tests was the bearing capacity of the wood infill walls. No vertical load was applied on the specimens. The lateral cyclic load was applied at the top of the wood wall and controlled by displacement following the loading protocol proposed by ISO 21581 (2010). The displacement time history was presented in Fig. 3. The reference displacement, Δ, was determined by the height of wood wall (denoted by H), as H/15 (ISO 21581 2010). Same reference displacement ($\Delta = 40$ mm, calculated from specimen 2) was used for the two specimens for the convenience of comparative analysis.

Figure 4 shows typical results in terms of upper horizontal displacement versus loading, i.e. hysteric curves and envelope curves. The hysteric curves were S-shaped. And obvious pinching behaviors were observed. It is principally caused by the slide between wood infill walls and exterior timber frames which is closely related to clearances induced by plastic deformations. The envelope curves exhibited clear nonlinearity and also could be simplified as a bilinear model before maximum load, i.e. elastic stage and plastic stage. The yield point was approximately determined by deformation rate method (Li et al. 2015; Xie et al.

Fig. 3 Loading protocol for the cyclic tests of wood infill walls

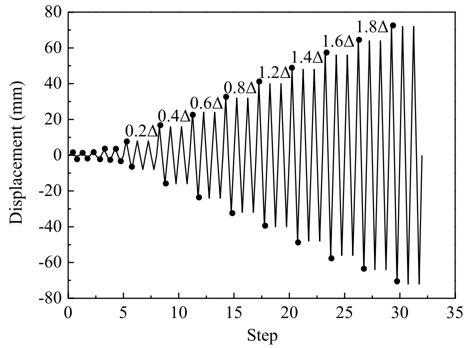

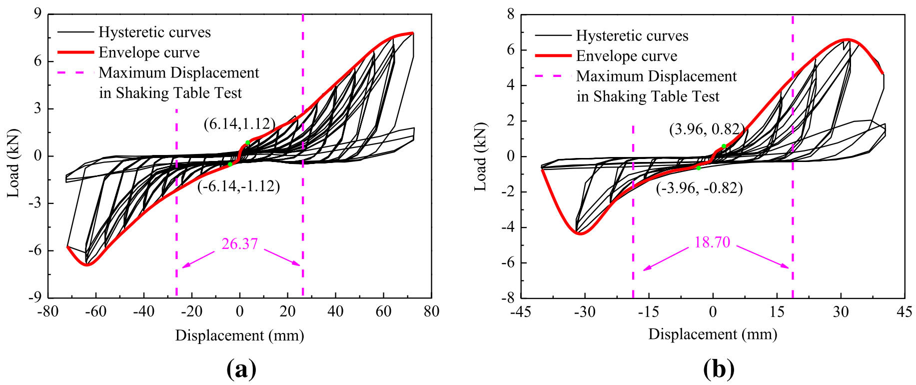

Fig. 4 Load–displacement curves: **a** Specimen 1; and **b** Specimen 2

Fig. 5 The final failure mode of wood infill walls: **a** Specimen 1; and **b** Specimen 2

2020a, b). The elastic stiffness and plastic stiffness of specimen 1 were 0.18 kN/mm and 0.11 kN/mm with a yield displacement of 6.14 mm, which were lower than that of specimen 2 (0.21 kN/mm and 0.15 kN/mm in elastic stage and plastic stage with a yield displacement of 3.96 mm). Tests were terminated with out of plane failure of wood infill walls at 72 mm and 40 mm for specimen 1 and specimen 2, respectively, as shown in Fig. 5.

Simultaneously, the bearing capacity decreased rapidly and was nearly close to 0, as shown in Fig. 4.

3 Description of the shaking table test

3.1 Model similitude factors

Shaking table test model must be able to reproduce dynamic behaviors of the prototype by use of three independent factors according to the similarity theory (Sabnis et al. 1983). The dimension scaling factor S_l was 1/6 considering the size limitation of the shaking table. According to the wood material test results, the scaling parameter of elastic modulus S_E was determined to 1.0. The acceleration scaling factor S_a was equal to 1.5 due to the limitation of total weight of additional mass in laboratory. Then other parameters were deduced by dimensional analysis, and the main factors are listed in Table 1.

3.2 Model construction

The test model, taking Xi'an Bell Tower as the prototype, represents a typical traditional timber structure in China. The model is a two-storey timber structure with additional corridor around the periphery at each storey, as shown in Fig. 6a. It is symmetric at the two principal axes, one of which in east–west direction was denoted as X-axis and the other was denoted as Y-axis, as shown in Fig. 6b, c. The total height of the model is 4.27 m, and that of the ground storey is 1.44 m. The columns and beams are connected by mortise-tenon joints with different styles (number 1–3 in Fig. 6a). And the columns are placed on the top of cornerstones by inserting small protruding tenons at the bottom into grooves in the cornerstones (number 4 in Fig. 6a). Dou-Gong (also called bracket complex) in different styles (number 5–8 in Fig. 6a), consisted of rectangular blocks (Dou) and bracket arms (Gong), are located on the surface of cover beams to support upper load. All the members were fabricated according to traditional practices adopted by the prototype structure. The cross section sizes of the main components were shown in Fig. 6b and c. Scotch pine (Pinus sylvestris) was used to make these components and the mechanical properties obtained from standard material properties tests (GB 1927 ~ 1943–91 1992) were listed in Table 2.

The wood infill walls as partition between outside principal columns were fabricated by wood-based composite board without considering the influence of doors and windows with

Table 1 Main similitude scaling factors of the model

Parameter	Relationship	Scaling factor	Remark
Length	S_l	1/6	Independent factor
Elastic modulus	$S_E = S_\sigma$	1	Independent factor
Stress	S_σ	1	
Acceleration	S_a	1.5	Independent factor
Density	$S_\sigma/(S_a \cdot S_l)$	4	
Mass	$(S_\sigma \cdot S_l^2)/S_a$	1/54	
Force	$S_\sigma \cdot S_l^2$	1/36	
Frequency	$S_l^{-0.5} \cdot S_a^{0.5}$	3	
Time	$S_l^{0.5} \cdot S_a^{-0.5}$	1/3	

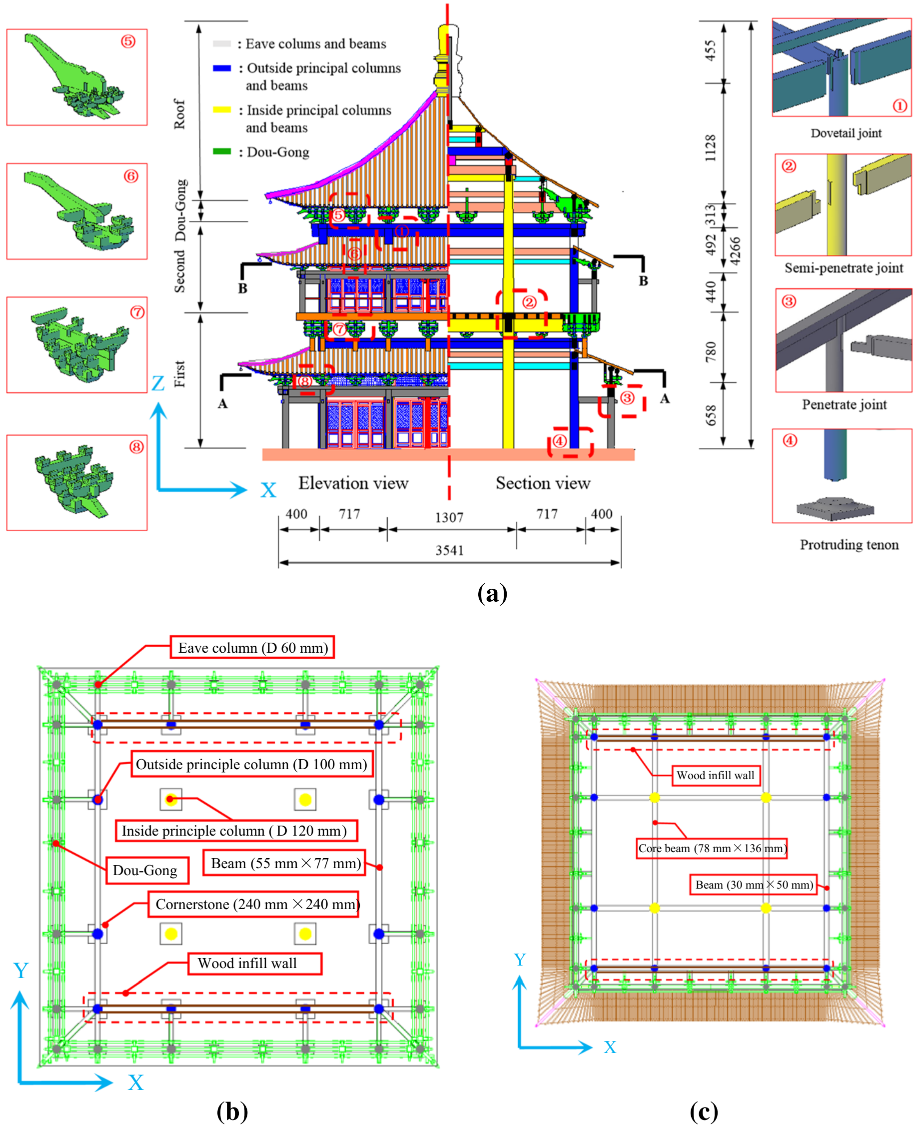

Fig. 6 Detailed information of the model (Xie et al. 2019): **a** Elevation and section views of the model; **b** Section A–A; and **c** Section B–B. *D* is the diameter of timber column

openings (as shown in Fig. 1) on the lateral stiffness in the model structure. Three specimens with the same aspect ratio were only installed in X direction in each storey to comparatively analyse the influence of wood infill walls to the overall structure, as shown in Fig. 7. The infill walls also have a ability to bear load out of plane, which is closely related to the connection between infill walls and frames. In order to minimize this impact, the connection between wood infill walls and timber frames only depended on friction without any connecting members.

Table 2 Mechanical properties of scotch pine

	Moisture content	Specific gravity (g/cm^3)	Parallel to Grain (MPa)			Perpendicular to Grain (MPa)		
			Compressive strength	Tension strength	Modulus of elastic	Compressive strength	Modulus of elastic (T)	Modulus of elastic (R)
Mean	11.2%	0.52	48.2	86.6	10,870	4.52	663	1043
CV (%)	2.67	7.33	4.89	4.86	17.21	2.70	13.37	19.28

T is the tangential direction and *R* is the radial direction

Fig. 7 The test model on the shaking table

In order to meet the requirement of mass similarity, a total of 5.84 tons additional mass with rectangular steel blocks (215 mm × 100 mm × 60 mm, 160 mm × 80 mm × 60 mm) were evenly fixed on the overhanging roofs (1.58 tons, 1.06 tons and 1.92 tons on first, second and top overhanging roof, respectively) and the floor panel of the second storey (1.28 tons). The complete test model is shown in Fig. 7.

3.3 Test procedure and measuring schemes

Considering the local soil condition, the dynamic characteristics of the structure and the specified acceleration response spectrum according to seismic code (Zhou and Lu 2016), three earthquake records were selected for testing: Lanzhou wave (artificial wave record), Kobe and Wenchuan waves (natural earthquake records). Figure 8 summarizes the acceleration response spectra of the selected earthquakes.

The acceleration amplitude and time duration of the waves were scaled considering the prescribed similitude scaling parameters. Table 3 lists the complete sequence of excitation. Five seismic hazard levels with peak ground acceleration (PGA) of 0.1 g (scaled PGA of

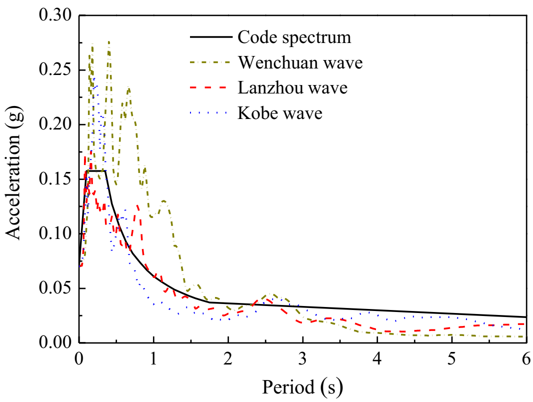

Fig. 8 The acceleration response spectra of the selected seismic inputs

Table 3 Test program

Phase	Test case	Case name	PGA (g)	Phase	Test case	Case name	PGA (g)
I	1	WN-I-XY	0.035	IV	18	L-IV-X	0.3
II	2	K-II-X	0.1		19	L-IV-Y	
	3	K-II-Y			20	W-IV-X	
	4	L-II-X			21	W-IVY	
	5	L-II-Y			22	WN-IV-XY	0.035
	6	W-II-X		V	23	K-V-X	0.6
	7	W-II-Y			24	K-V–Y	
	8	WN-II-XY	0.035		25	L-V-X	
III	9	K-III-X	0.2		26	L-V–Y	
	10	K-III-Y			27	W-V-X	
	11	L-III-X			28	W-VY	
	12	L-III-Y			29	WN-V-XY	0.035
	13	W-III-X		VI	30	K-VI-X	0.93
	14	W-III-Y			31	L-VI-X	
	15	WN-III-XY	0.035		32	W-VI-X	
IV	16	K-IV-X	0.3		33	WN-VI-XY	0.035
	17	K-IV-Y			–	–	–

K, L, and W represent the earthquake of Kobe, Lanzhou and Wenchuan, respectively; X and Y are the directions of the input earthquake, respectively

frequent earthquake of intensity 8, described in the *Code for Seismic Design of Buildings of China* (GB 50,011–2010 2010)), 0.2 g (frequent earthquake of intensity 9), 0.3 g (design earthquake of intensity 8), 0.6 g (rare earthquake of intensity 8 or design earthquake of intensity 9) and 0.93 g (rare earthquake of intensity 9) were carried out. White noises with the PGA of 0.035 g were inputted between the intervals of the seismic hazard levels to identify the changes of the dynamic characteristics. In the case of 0.6 g, deformation in Y direction without wood infill walls was too large approaching to collapse. In order to prevent the model from collapsing, only excitation in X direction was conducted at the PGA of 0.93 g.

Acceleration and displacement sensors were used to accurately capture responses of interest. In total, 20 accelerometers and 10 displacement sensors were installed on the model according to the layout shown in Fig. 9.

4 Experimental results and discussion

4.1 Damage patterns

In the case of minor earthquakes (below the PGA of 0.2 g), no difference in deformation was observed between the two directions. With the gradual increase of PGA, deformation in the Y direction was obviously larger than that in the X direction. The main reason is that there was no wood infill wall to provide additional stiffness to resist lateral forces in the Y direction. When the PGA reached 0.6 g, obvious incline deformation was observed

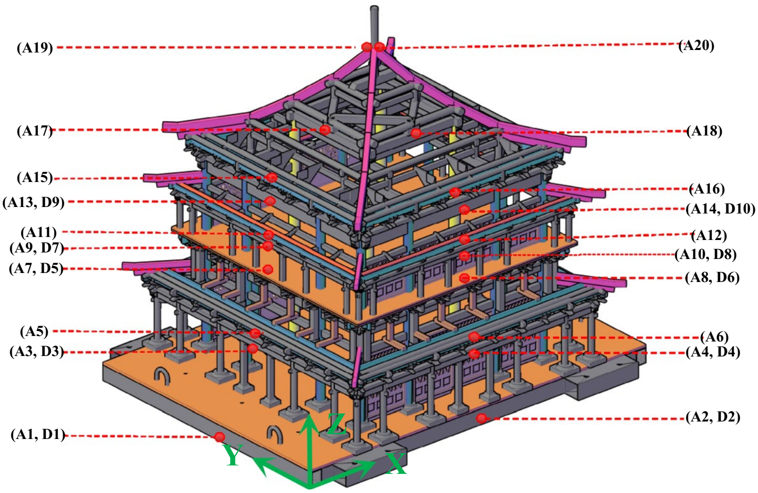

Fig. 9 Arrangement of measuring points. Letters A and D represent the accelerometer and displacement transducers, respectively

in the Y direction (the maximum inter-storey drift reached up to 1/52 approaching to the threshold value (1/30) of severe damage defined by Katagihara (2001)). Then earthquake waves were only applied to X direction. Up to the end of 0.93 g, no substantial damage was observed in both directions, except some slight pulled-out tenons in mortise-tenon joints, some minor damages in Dou-gongs and extrusion deformations in sparrows, as shown in Fig. 10. In addition, some wood infill walls in the X direction collapsed out of plane. Similarly, the collapse phenomena of wood infill walls were also observed in other traditional timber structures (Xue and Xu 2018) and actual structures (Zhou et al. 2010). It is indicated that wood infills wall can act as the first line of defense against earthquake.

4.2 Influence of wood infill walls on dynamic characteristics

Dynamic identification was carried out by white noise before and after each seismic hazard level, aiming at evaluating the variation of dynamic characteristics. Based on transfer functions of measuring points resulting from white noises, the dynamic characteristics, including natural frequency and damping ratio, were obtained (Xie et al. 2019).

The Fourier spectra established by transfer functions based on the responses of WN-I-XY excitation are shown in Fig. 11. The natural frequencies in the original state without damage were 2.85 Hz in X direction and 2.23 Hz in Y direction. Figure 12a illustrates the variation trend of natural frequency with seismic intensity. It can be seen that the frequencies in both direction decreased with the increase of the PGA. It is principally because the stiffness decreased due to cumulative damage. The fundamental frequency in X direction remained basically unchanged (2.85–2.77 Hz) with a low decrease less than 3% during the PGA of 0–0.2 g indicating that no damage almost occurred, which was consistent with the observed phenomena during tests. As the PGA gradually increased to 0.6 g, the model was subjected to stronger earthquakes, resulting in 11% decrease from 2.77 to 2.46 Hz in X direction which demonstrated that minor damage had occurred. However, the frequency in Y direction decreased rapidly and was only 1.76 Hz at the PGA of 0.6 g, 21% reduction with respect to the initial frequency. In addition, it is obvious that the frequencies in X

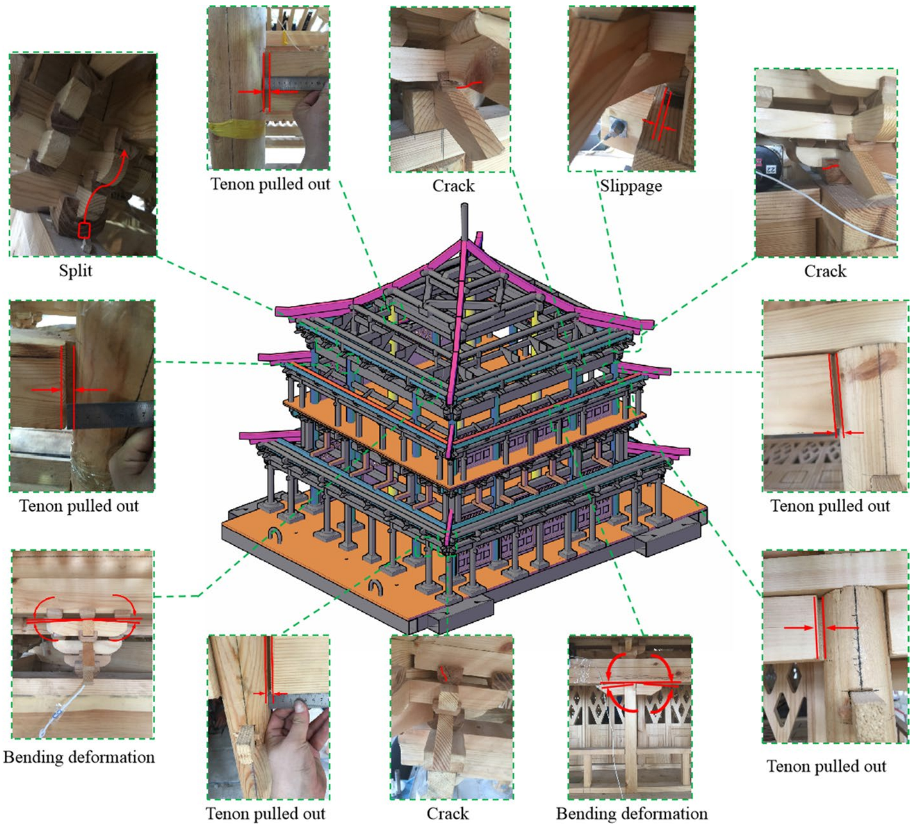

Fig. 10 Damage patterns of the model

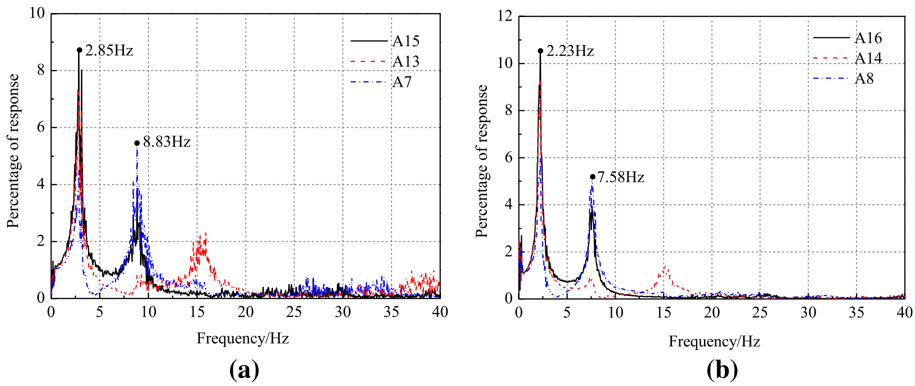

Fig. 11 Fourier spectra of different measuring points under WN-I-XY: **a** X direction; and **b** Y direction. The first and second peak points in the Fourier spectra are the frequencies of first-order and second-order, respectively., respectively

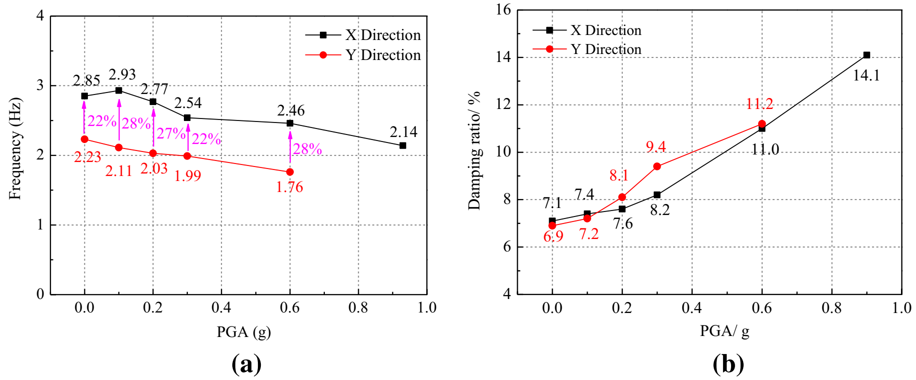

Fig. 12 Comparison of dynamic characteristics: **a** frequency; and **b** damping ratio

direction were significantly greater than those in Y direction with 25% higher on average. Even at the PGA of 0.93 g, the frequency (2.15 Hz) in X direction was still close to 96% of the initial frequency in Y direction. It is indicated that wood infill walls can effectively improve the natural frequency of the structure.

By comparison of the damping ratios between the two directions (shown in Fig. 12b), it can be seen that the damping ratios in X direction were slightly higher than that in Y direction in the initial state due to the wood infill walls which is also regard as a additional source of structure damping. However, with the increasing amplitude of earthquake inputs, the damping ratio was gradually smaller than that in Y direction during the PGA of 0.2–0.6 g. The contributing factor is that with the increase of earthquake intensity, more serious damage in Y direction led to greater increase of damping constant and larger degradation of structural stiffness. And according to the theory of viscous damping (Chopra 2001), the damping ratio is proportional to damping constant and inversely proportional to structural stiffness. Therefore, the increase of damping ratio caused by structural damage exceeded that provided by wood infill walls. Subsequently, when the PGA reached 0.6 g, although the damping ratio was also 0.2% lower than that in Y direction, the rate of increment had already been significantly larger than that in Y direction. It is indicated that significant damage began to form in X direction. Therefore, it can be predicted from the overall development trend of the damping ratio (Fig. 12b) that damping ratio in X direction will be significantly greater than that in Y direction under larger earthquakes, such as at the PGA of 0.93 g. A similar phenomenon also was found in a traditional column-and-tie timber structure carried out by Xue and Xu (2018).

4.3 Influence of wood infill walls on stiffness

Equivalent inter-storey stiffness, which is derived from hysteresis loop (inter-storey shear force versus relative displacement) of white noise by linear regression analyses assuming a zero intercept (Wu et al. 2018a), was often used to estimate the lateral resistance of a structure. Figure 13 illustrates the hysteretic curves of the first and second storeys in both directions computed by the test data of the WN-I-XY excitation. Based on this, the differences of equivalent inter-storey stiffness between the two directions of the first and second storeys were obtained with the values of 0.71 kN/mm

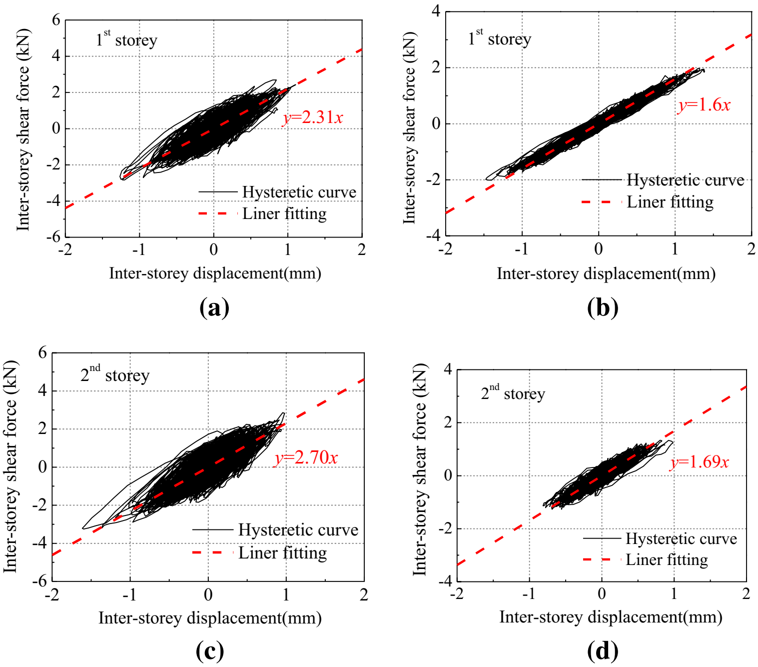

Fig. 13 Inter-story shear force–displacement hysteretic curves: **a** X direction of first storey; **b** Y direction of first storey; **c** X direction of second storey; and **d** Y direction of second storey

and 1.01 kN/mm at the initial stage, respectively, which were basically equal to storey stiffness of the wood infill walls (0.72 kN/mm and 0.84 kN/mm, calculated by accumulating all the stiffness of wood infill walls with the same aspect ratio in each storey). It is indicated that the equivalent inter-storey stiffness can reasonably reflect the lateral resistance of a structure. Figure 14 shows the degradation of the equivalent inter-storey stiffness in both directions. The inter-storey stiffness decreased drastically during the PGA of 0–0.2 g in the first and second storeys in X direction. One possible reason for this is that the wood infill walls in X direction also act as the first line of defense against earthquake. Under earthquakes in earlier stages, the wood infill walls squeezed

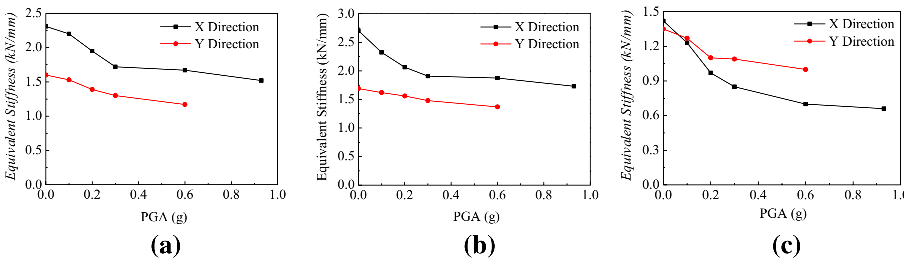

Fig. 14 The degradation curves of equivalent inter-storey stiffness: **a** first storey; **b** second storey; and **c** dou-gong storey

with beams and columns resulting in irreversible extrusion deformations at contact surfaces. Eventually, gaps that resulted from irreversible extrusion deformations mentioned above between walls and beams or columns led to a rapid decrease in stiffness. Subsequently, the stiffness in X direction dropped slowly during the PGA of 0.3–0.6 g. One primary reason is that the stiffness of wood infill walls were basically unchanged after the displacement (6.65 mm in the first storey and 5.43 mm in the second storey under the PGA of 0.3 g, as shown in Fig. 18) exceeded a certain value i.e. the yield points of the wood infill walls (6.14 mm in the first storey and 3.96 mm in the second storey, as shown in Fig. 4). When the PGA reached 0.6 g, the stiffness of the first storey and second storey in X direction were 1.67 kN/mm and 1.87 kN/mm, 43% and 37% greater than that in Y direction, respectively. And the degradation rate of the stiffness in X direction was less than that in the other direction during the PGA of 0.3–0.6 g. In the case of the PGA reached 0.93 g, the equivalent inter-storey stiffness (1.52 kN/mm in the first storey and 1.73 kN/mm in the second storey) in X direction was still higher than that (1.17 kN/mm in the first storey and 1.37 kN/mm in the second storey) in Y direction with the PGA of 0.6 g. In addition, the stiffness of Dou-Gong in X direction was almost equal to that in Y direction at the initial state due to the same structural form and arrangement. With the increase of the input seismic intensity, the reduction of the stiffness in X direction was obviously greater than that in Y direction (as shown in Fig. 14c). It is principally because that the stiffness of the structure below Dou-Gong storey in X direction is significantly larger than that in Y direction (as shown in Fig. 14a, b), which led to obviously stronger structural response in corresponding Dou-Gong storey (as shown in Fig. 18a, b) resulting in more serious damage. Therefore, it demonstrated that the wood infill walls not only can significantly increase the lateral stiffness of the corresponding storey, but also has an significant influence on the variation in stiffness of adjacent storey under earthquake.

The fundamental relation of national frequency *f*, generalized mass *M*, and structural stiffness *K* of a single degree of freedom system (Chopra 2001) is expressed as follow:

$$f = \frac{\sqrt{K/M}}{2\pi} \tag{1}$$

Assuming that the mode shapes change little during testing, the degradation factor γ of the overall stiffness can be approximately calculated as Eq. (2) (Vieux-Champagne et al. 2017):

$$\gamma = \frac{K_0 - K}{K_0} = 1 - \left(f/f_0\right)^2 \tag{2}$$

where K_0 and K are the initial stiffness and the stiffness after test, respectively. f_0 and f are the frequencies corresponding to K_0 and K. Figure 15 shows the degradation factors of the overall stiffness of the model in both directions. It can be seen that the degradation amplitude of the stiffness in Y direction was obviously larger that in X direction. When the PGA reached 0.6 g, the stiffness in Y direction decreased about 38%, while only 25% in X direction. In the case of the PGA reached 0.93 g, the degradation amplitude of the stiffness in X direction suddenly increased. It is relevant to the phenomenon that some wood infill walls were fell down out of plane, and the tenons were also noticeably pulled out from mortise due to the reduced constraint from wood infill walls.

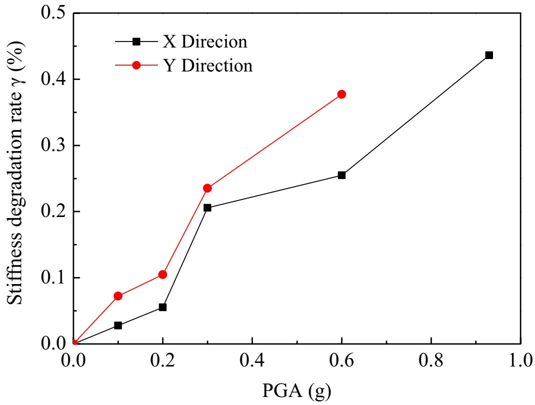

Fig. 15 The degradation factor curves of overall stiffness

4.4 Influence of wood infill walls on acceleration response

Test results showed that the acceleration responses of the model were similar under the three earthquakes. Therefore, the acceleration responses excited by Wenchuan wave were only analyzed as an example. Figure 16 represents the peak accelerations of different storeys in X and Y directions. It was found that under the same PGA, the peak accelerations at the first and second storeys in X direction were obviously greater than those at the similar locations in Y direction. One primary reason is that the wood infill walls restricted the rotation of mortise-tenon joints resulting in reduction in energy dissipation. Meanwhile, the relatively smaller deformation in X direction (as shown in Fig. 18) due to the increased stiffness also restricted the full use of energy dissipation ability of wood infill walls. Furthermore, in the case of severe earthquakes (0.3–0.6 g), the increasing rates of the peak accelerations at these locations in X direction were close to that in Y direction. It reveals that significant deformation in wood infill

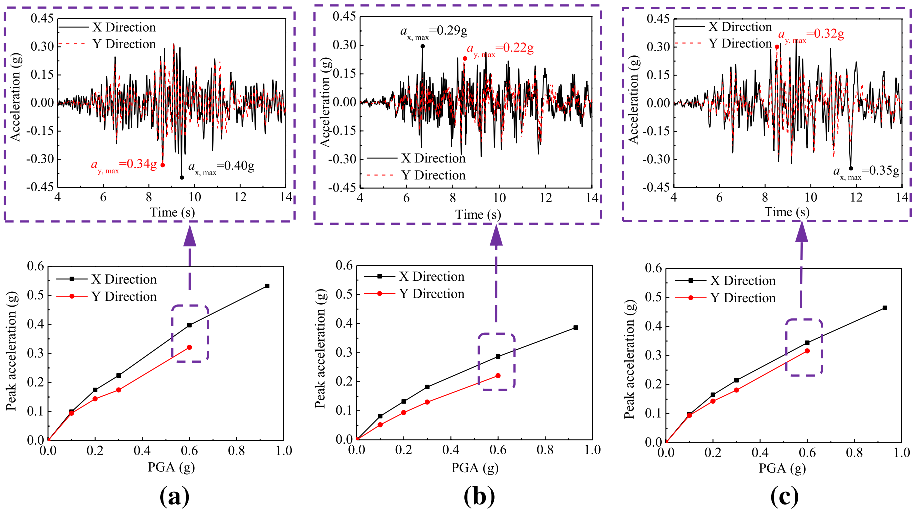

Fig. 16 Peak accelerations at different measuring points under Wenchuan wave: **a** first storey; **b** second stroey; and **c** dou-gong storey

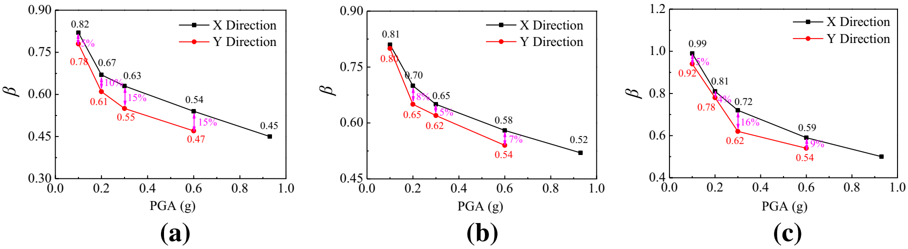

Fig. 17 Acceleration magnification factors of the model at roof: **a** Kobe; **b** Lanzhou; and **c** Wenchuan

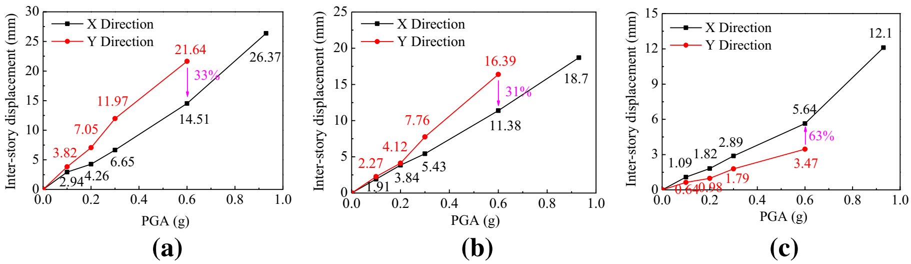

Fig. 18 Inter-storey displacement at different measuring points under Wenchuan wave: **a** first storey; **b** second storey; and **c** dou-gong storey

walls due to the structure damage is able to greatly weaken the structure acceleration response. In addition, the peak accelerations at the Dou-Gong storey also had the similar trend, namely the peak accelerations in X direction were greater than that in Y direction, due to the large ones of adjacent storey (the second storey) in the same direction.

The acceleration amplification factor β is usually used to evaluate the shock absorption of a structure (Xue and Xu 2018). It is defined as the ratio of peak acceleration between the top of the structure (roof storey) and the shaking table. The acceleration amplification factors of the roof storey under different earthquakes are plotted in Fig. 17. It can be seen that the acceleration amplification factors in X direction were always larger than that in Y direction, as expect, which is mainly due to the effect of wood infill walls. This fact proved that the wood infill walls can not only increase the stiffness of corresponding storey, but also enhance the structural integrity resulting in increase in overall stiffness. In addition, the acceleration amplification factors in X directions were always less than 1.0, which were similar to other traditional timber structures without wood infill walls (Zhang et al. 2011; Song et al. 2017; Xue and Xu 2018; Xie et al. 2019). Also, the differences of the acceleration amplification factors in both directions were relatively small with a maximum value of 16% at the PGA of 0.3 g under Wenchuan wave. It indicated that the shock absorption capacity of the traditional timber structure is less susceptible by wood infill walls.

4.5 Influence of wood infill walls on displacement response

The maximum relative displacements in both directions of each storey under Wenchuan wave are plotted in Fig. 18. It was found that the maximum relative displacements of the first and second storeys in X direction were lower than those in Y direction due to the increased stiffness resulting from wood infill walls. In addition, the maximum relative displacement of the two storeys in X direction almost changed linearly. These implied that the stiffness of structure without wood infill walls degraded severely due to the serious damage under the same earthquake. In the case of the PGA of 0.93 g, the maximum inter-storey displacement were 26.37 mm and 18.7 mm in the first and second storeys (Fig. 18a, b) in X direction, whereas from the cyclic tests, an ultimate value of 72 mm and 40 mm were found (Fig. 4a, b). It is indicated that the structure in X direction was less damaged, far from the limits of severe damage. However, as for the Dou-Gong storey, the maximum relative displacements in the X direction were noticeably bigger than that in the other direction (Fig. 18c). It implied that the degradation of the stiffness in X direction was more serious than that in Y direction, as shown in Fig. 14c.

4.6 Influence of wood infill walls on energy dissipation

The energy-based evaluation method considered the contributions of various energy terms during earthquakes is also used to evaluate the seismic performance of a structure. It is initiated by Zahrah (1982) and given in Eq. (3).

$$E_{\mathrm{I}} = E_{\mathrm{K}} + E_{\xi} + E_{\mathrm{E}} + E_{\mathrm{P}} \tag{3}$$

where E_{I} is the relative total energy (Uang and Bertero 1990); E_{K} is the kinetic energy; E_{ξ} is the damping energy; E_{E} is the elastic strain energy; E_{P} is the hysteretic (irrecoverable plastic strain) energy.

E_{K} and E_{E} transformed each other over time during excitation and vanished at the end of vibration, which are related to instant response of a structure. In addition, they are negligibly small compared with E_{ξ} and E_{P} (Shen and Akbaş 1999). Thus, the total input seismic energy approximately appears in the form of damping energy E_{ξ} and plastic strain energy E_{P}, as following:

$$E_{\mathrm{I}} \cong E_{\xi} + E_{\mathrm{P}} \tag{4}$$

The energy input E_{I} can be easily calculated by Eq. (5) from masses m_i, relative displacement x_i, and acceleration $\ddot{x}_{\mathrm{g}}$ of the shaking table. However, it is not possible to accurately calculate E_{ξ} due to the complex mechanism of damping. In order to effectively assess E_{ξ}, viscous damping model was usually used. First, the tested structure was idealized as a multi-particle model with three lumped masses (The top roof placed on the Dou-Gong storey was also regard as a rigid body, so the Dou-Gong storey and the top roof were simplified into a concentrated mass), as shown in Fig. 19. Then, the viscous damping of the structure was represented by the traditional Rayleigh damping matrix, which applied the frequencies related to the first and second vibration modes (Benavent-Climent et al. 2014a, b) and adopted the same damping ratio ξ for both modes obtained from the shaking table tests. Finally, E_{ξ} was determined by Eq. (6).

$$E_{\mathrm{I}} = -\int_0^t \{\dot{x}\}^{\mathrm{T}}[M]\{\ddot{x}_{\mathrm{g}}\}\mathrm{d}t = -\sum_{i=1}^{n}\int_0^t m_i\ddot{x}_{\mathrm{g}}\dot{x}_i\mathrm{d}t \tag{5}$$

$$E_{\xi} = \int_0^t \{\dot{x}\}^{\mathrm{T}}[C]\{\dot{x}\}\mathrm{d}t \tag{6}$$

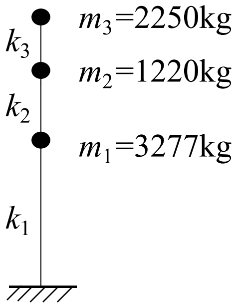

Fig. 19 Lumped mass model

The total energy E dissipated by a structure was equal to the energy input E_I during an earthquake. Table 4 lists the energy dissipation in the two directions under earthquakes. It is clear that the total dissipated energy in X direction was relatively smaller than that in Y direction. It is principally because that wood infill walls restricted the rotation of mortise-tenon joints, which are the key elements to dissipate energy in traditional timber structures (Zhang et al. 2011). However, when the PGA was up to 0.6 g under Wenchuan wave, energy dissipation in X direction was obviously larger than that in the other direction, increased by nearly 25%. It is indicated that the wood infill walls, regarded as a source of damping, may contribute to the total energy dissipation of traditional timber structure only when experiencing significant damage.

In addition, the E_ξ/E_I ratios were given in Fig. 20, which reflected the dependency of the damping energy on the structural responses. Generally, the ratios in both direction were only slightly less than 1 at initial stage and reduced rather quickly as the PGA increasing. When the structure was mainly in elastic range, the damping energy E_ξ played a dominant role in dissipating input energy E_I. As the structure suffered larger inelastic deformation under stronger earthquakes, the plastic strain energy E_P, which is considered to be the major contribution to the damage of a structure, dissipated more from E_I, and E_ξ became less. Moreover, Fig. 20 also reflected that the wood infill walls significantly reduced the decline rate of E_ξ/E_I. When the PGA was 0.6 g, the average value in the X direction was close to 63% in X direction, larger than that with the value of 41% in Y direction. Even though the PGA reached 0.93 g, the damping energy E_ξ still occupied 40% of the total energy in X direction. The reason for less damage of the traditional timber structure with wood infill walls was revealed from the energy dissipation

Table 4 Energy dissipation in the two directions (unit: N·m)

Earthquake	Direction	PGA				
		0.1 g	0.2 g	0.3 g	0.6 g	0.93 g
Kobe	X	11	38	128	768	1323
	Y	18	82	248	1013	–
Lanzhou	X	36	98	194	732	1524
	Y	26	180	354	1013	–
Wenchuan	X	81	144	305	1283	2750
	Y	53	160	330	1029	–

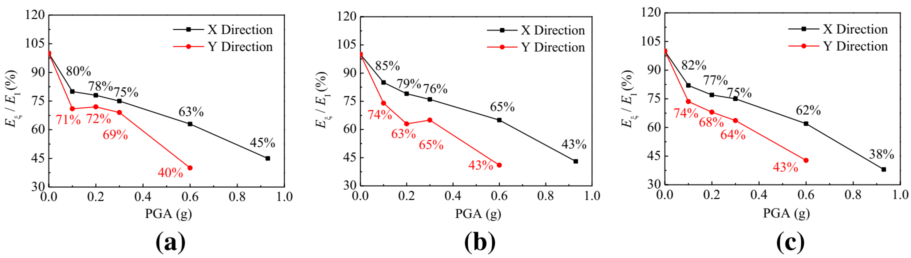

Fig. 20 Variation of E_ξ/E_I in both directions: **a** Kobe; **b** Lanzhou; and **c** Wenchuan

mechanism, i.e. traditional timber structure with wood infill walls is less vulnerable to damage compared with that without ones.

5 Conclusion

Static tests and shaking table tests have been conducted on 1:6 scaled specimens (wood infill walls) and model (a traditional timber structure with wood infill walls installed only in one direction), respectively. The contribution of wood infill walls to the seismic performance in term of dynamic properties, dynamic responses, equivalent stiffness and energy dissipation were discussed and quantified. Based on the tests and comparison results, the following conclusions were obtained:

1. Wood infill walls can enhance the earthquake resilience of traditional timber structure as the structure without ones suffered greater inter-storey deformation and it was vulnerable to collapse under severe earthquakes.
2. Wood infill walls in traditional timber structure obviously increase the natural frequency of the structure and effectively reduce the decaying rate of frequency under earthquakes. As a source of structure damping, the wood infill walls can improve the damping ratio of the structure before the earthquake. However, with the increase of earthquake intensity, the gradually accumulated structural damage may contribute to more damping ratio than that provided by wood infill walls.
3. Wood infill walls effectively increase the stiffness of corresponding storey, resulting in reduction in displacement response and increase in acceleration response under earthquakes. Also, it aggravates the damage of adjacent structural storey without wood fill walls, resulting in reduction in stiffness and increase in inter-storey displacement.
4. Under minor earthquakes, the energy dissipation of the traditional timber structure with wood infill walls was slightly weakened due to the restrict rotation of mortise-tenon joints resulting from wood infill walls. Only in the case of large deformation can the wood infill walls contribute to the total energy dissipation of the structure.
5. The distribution of E_I between E_ξ and E_P is significantly affected by the characteristics of structure. The wood infill walls as a source of damping increase the proportion of damping energy dissipation in total energy and decreased the proportion of plastic strain energy related to structure damage.

Acknowledgements The authors gratefully acknowledge the funding support received from the National Key Research and Development Program (Grant No. 2017YFC0703507) and the National Natural Science Foundation of China (Grant No. 51878550).

Compliance with ethical standards

Conflict of interest The authors declare that they have no conflicts of interest to this work.

References

Benavent-Climent A, Escolano-Margarit D, Morillas L (2014a) Shake-table tests of a reinforced concrete frame designed following modern codes: seismic performance and damage evaluation. Earthquake Engng Struct Dyn 43(6):791–810

Benavent-Climent A, Morillas L, Escolano-Margarit D (2014b) Seismic performance and damage evaluation of a reinforced concrete frame with hysteretic dampers through shake-table tests. Earthquake Engng Struct Dyn 43(15):2399–2417

Benavent-Climent A, Ramirez-Marquez A, Pujol S (2018) Seismic strengthening of low-rise reinforced concrete frame structures with masonry infill walls: Shaking-table test. Eng Struct 165:142–151

Branco JM, Gonçalves A, Guerreiro L, Ferreira J (2014) Cyclic behavior of composite timber-masonry wall in quasi-dynamic conditions reinforced with superelastic damper. Constr Build Mater 52:166–176

Chang WS, Komatsu K, Hsu MF, Chen WJ (2007a) On mechanical behavior of traditional timber shear wall in Taiwan I: background and theory derivation. J Wood Sci 53(1):17–23

Chang WS, Hsu MF, Komatsu K, Chen WJ (2007b) On mechanical behavior of traditional timber shear wall in Taiwan II: simplified calculation and experimental verification. J Wood Sci 53(1):24–30

Chang WS, Shanks J, Kitamori A, Komastsu K (2009) The structural behaviour of timber joints subjected to bi-xial bending. Earthquake Engng Struct Dyn 38(6):739–757

Chen CC, Qiu HX, Lu Y (2016) Flexural behaviour of timber dovetail mortise-tenon joints. Constr and Build Mater 112:366–377

Chopra A (2001) Dynamics of structures: theory and applications to earthquake engineering, 3rd edn. Prentice Hall, Upper Saddle River

Chun Q, Meng Z, Han Y (2017) Research on mechanical properties of main joints of Chinese traditional timber buildings with the type of post-and-lintel construction. Int J Archit Herit 11(2):247–260

Crayssac E, Song XB, Wu YJ, Li K (2018) Lateral performance of mortise-tenon jointed traditional timber frames with wood panel infill. Eng Struct 161:223–230

D'Ayala DF, Tsai PH (2008) Seismic vulnerability of historic Dieh-Dou timber structures in Taiwan. Eng Struct 30(8):2101–2113

Dutu A, Sakata H, Yamazaki Y, Shindo T (2015) In-plane behavior of timber frames with masonry infills under static cyclic loading. J Struct Eng 142(2):04015140

GB 1927–1943–91 (1992) Testing methods for physical and mechanical properties of wood. Architecture and Building Press, Chinese Academy of Forestry, Beijing

GB 50011-2010 (2010) Code for seismic design of buildings. China Architecture & Building Press, Beijing

He JX, Wang J (2018) Theoretical model and finite element analysis for restoring moment at column foot during rocking. J Wood Sci 64(2):97–111

ISO 21581 (2010) Timber structures–static and cyclic lateral load test methods for shear walls. International Organization for Standardization, Geneva

Katagihara K (2001) Preservation and seismic retrofit of the traditional wooden buildings in Japan. J Temp Design Arch Environ 1(1):12–20

King WS, Yen JYR, Yen YNA (1996) Joint characteristics of traditional Chinese wooden frames. Eng Struct 18(8):635–644

Kitamor A, Jung K, Hassel I, Chang W, Komatsu K, Suzuki Y (2010) Mechanical analysis of lateral loading behavior on Japanese traditional frame structure depending on the vertical load. In: 11th World Conference on Timber Engineering, Riva del Garda, Italy

Li X W, Zhao J H, Ma GW, Chen W (2015) Experimental study on the seismic performance of a double-span traditional timber frame. Eng Struct 98:141–150

Qin SJ, Yang N (2018) Dai L (2018) Rotational behavior of column footing joint and its effect on the dynamic characteristics of traditional Chinese timber structure. Shock Vib 8:1–13

Sabnis GM, Harris HG, White RN, Mirza MS (1983) Structural modeling and experimental techniques. Prentice-Hall, Englewood Cliffs

Shi XW, Chen YF, Chen JY, Yang QS, Li TY (2018) Experimental assessment on the hysteretic behavior of a full-scale traditional Chinese timber structure using a synchronous loading technique. Adv Mater Sci Eng 1:1–15

Shen J, Akbaş B (1999) Seismic energy demand in steel moment frames. J Earthq Eng 3(04):519–559

Suzuki Y, Maeno M (2006) Structural mechanism of traditional wooden frames by dynamic and static tests. Struct Control Health Monit 13(1):508–522

Song XB, Wu TJ, Li L, Gu XL (2017) Shaking table test on a traditional pavilion-style wooden pagoda. J Build Struct 38(2):10–19

Tsuwa I, Koshihara M (2012) A study on the effect of wall stiffness on the vibration characteristics of traditional timber frames including Kumimono. Institute of Industrial Science, University of Tokyo, Bulletin of ERS:45.

Uang CM, Bertero VV (1990) Evaluation of seismic energy in structures. Earthquake Engng Struct Dyn 19(1):77–90

Vieux-Champagne F, Sieffert Y, Grange S, Polastri A, Ceccotti A, Daudeville L (2014) Experimental analysis of seismic resistance of timber-framed structures with stones and earth infill. Eng Struct 69:102–115

Vieux-Champagne F, Sieffert Y, Grange S, Nko'ol CB, Bertrand E, Duccini JC, Daudeville L (2017) Experimental analysis of a shake table test of timber-framed structures with stone and earth infill. Earthquake Spectra 33(3):1075–1100

Wu YJ, Song XB, Gu XL, Luo L (2018a) Dynamic performance of a multi-story traditional timber pagoda. Eng Struct 159:277–285

Wu YJ, Song XB, Li K (2018b) Compressive and racking performance of eccentrically aligned dou-gong connections. Eng Struct 175:743–752

Xie QF, Wang L, Zhang LP, Hu WB, Zhou TG (2019) Seismic behaviour of a traditional timber structure: shaking table tests, energy dissipation mechanism and damage assessment model. Bull Earthquake Eng 17(3):1689–1714

Xie QF, Wang L, Zhang LP, Xiang W, Hu WB (2020a) Rotational behaviours of fork-column Dou-Gong: experimental tests and hysteresis model. J Perform Constr Facil 34(3):04020032

Xie QF, Zhang LP, Miao Z, Zhou WJ (2020b) Li SY (2020) Lateral behavior of traditional Chinese timber frames strengthened with shape memory alloy: experiments and analytical model. J Struct Eng 146(6):04020083

Xu QF, Liu Q, Zhang FW, Gong CC (2015) Experimental research on seismic performance of mortise-tenon joint wood frame with brick masonry infilled wall. Build Struct 45(6):50–52

Xue JY, Xu D (2018) Shake table tests on the traditional column-and-tie timber structures. Eng Struct 175:847–860

Yeo SY, Komatsu K, Hsu MF, Chung YL, Chang WS (2018) Structural behavior of traditional Dieh-Dou timber main frame. Int JArchit Herit 12(4):555–577

Yeo SY, Komatsu K, Hsu MF, Que Z (2016) Mechanical model for complex brackets system of the Taiwanese traditional Dieh-Dou timber structures. Adv Struct Eng 19(1):65–85

Yuan JL (2018) Seismic analysis method considering wall participation for ancient timber frame buildings. J Build Struct 39(9):45–52

Zahrah TF (1982) Seismic energy absorption in simple structures. Ph.D. Dissertation, University of Illinois at Urbana-Champaign, Illinois.

Zhang XC, Xue JY, Zhao HT, Sui Y (2011) Experimental study on Chinese ancient timber-frame building by shaking table test. Struct Eng Mech 40(4):46–47

Zhou Q, Yan WM, Yang XS, Ji JB (2010) Earthquake damage to ancient buildings caused by Wenchuan earthquake. Sci Conserv Archaeol 22(1):37–45

Zhou Y, Lu XL (2016) Method and technology for shaking table model test of building structures. Science Press, Beijing